

# Specific labeling of synaptic schwann cells reveals unique cellular and molecular features

Ryan Castro<sup>1,2,3</sup>, Thomas Taetzsch<sup>1,2</sup>, Sydney K Vaughan<sup>1,2</sup>, Kerilyn Godbe<sup>4</sup>, John Chappell<sup>4</sup>, Robert E Settlage<sup>5</sup>, Gregorio Valdez<sup>1,2,6\*</sup>

<sup>1</sup>Department of Molecular Biology, Cellular Biology, and Biochemistry, Brown University, Providence, United States; <sup>2</sup>Center for Translational Neuroscience, Robert J. and Nancy D. Carney Institute for Brain Science and Brown Institute for Translational Science, Brown University, Providence, United States; <sup>3</sup>Neuroscience Graduate Program, Brown University, Providence, United States; <sup>4</sup>Fralin Biomedical Research Institute at Virginia Tech Carilion, Roanoke, United States; <sup>5</sup>Department of Advanced Research Computing, Virginia Tech, Blacksburg, United States; <sup>6</sup>Department of Neurology, Warren Alpert Medical School of Brown University, Providence, United States

**Abstract** Perisynaptic Schwann cells (PSCs) are specialized, non-myelinating, synaptic glia of the neuromuscular junction (NMJ), that participate in synapse development, function, maintenance, and repair. The study of PSCs has relied on an anatomy-based approach, as the identities of cell-specific PSC molecular markers have remained elusive. This limited approach has precluded our ability to isolate and genetically manipulate PSCs in a cell specific manner. We have identified neuron-glia antigen 2 (NG2) as a unique molecular marker of S100β+ PSCs in skeletal muscle. NG2 is expressed in Schwann cells already associated with the NMJ, indicating that it is a marker of differentiated PSCs. Using a newly generated transgenic mouse in which PSCs are specifically labeled, we show that PSCs have a unique molecular signature that includes genes known to play critical roles in PSCs and synapses. These findings will serve as a springboard for revealing drivers of PSC differentiation and function.

\*For correspondence: gregorio\_valdez@brown.edu

**Competing interests:** The authors declare that no competing interests exist.

**Funding:** See page 14

**Received:** 08 April 2020

**Accepted:** 08 June 2020

**Published:** 25 June 2020

**Reviewing editor:** Beth Stevens, Boston Children's Hospital, United States

© Copyright Castro et al. This article is distributed under the terms of the [Creative Commons Attribution License](https://creativecommons.org/licenses/by/4.0/), which permits unrestricted use and redistribution provided that the original author and source are credited.

## Introduction

The neuromuscular junction (NMJ) is a tripartite synapse comprised of an  $\alpha$ -motor neuron (the presynapse), extrafusal muscle fiber (the postsynapse), and specialized synaptic glia called perisynaptic Schwann cells (PSCs) or terminal Schwann cells. Due to its large size and accessibility, extensive research of the NMJ has been essential to the discovery of the fundamental mechanisms that govern synaptic function, including the concepts of neurotransmitter release, quantal transmission, and active zones, among others (*Katz and Miledi, 1967; Fatt and Katz, 1952; Sealock et al., 1989; Sobel et al., 1979; Sobel et al., 1977; Sanes and Lichtman, 1999; Darabid et al., 2014; Katz and Miledi, 1966; Robertson, 1956; Changeux et al., 1970; Godfrey et al., 1984; Jennings et al., 1993; Lwebuga-Mukasa et al., 1976; Nitkin et al., 1987; Porter and Froehner, 1983*). Likewise, the concept of glia that exist primarily to support synapse function, and thus the realization that synapses are tripartite, has its origins at the NMJ (*Robertson, 1956; Couteaux, 1960; Kang et al., 2007; Zuo et al., 2004; Griffin and Thompson, 2008; Boeke, 1949; Heuser and Reese, 1973; Miledi and Slater, 1968; Miledi and Slater, 1970; Peper et al., 1974; Astrow et al., 1994; Astrow et al., 1998; Reynolds and Woolf, 1992; Young et al., 2005*). PSCs surround the NMJ

where they are closely associated with its pre- and postsynaptic components (*Griffin and Thompson, 2008; Ko and Robitaille, 2015; Darabid et al., 2014*). In addition to providing trophic support for the NMJ (*Griffin and Thompson, 2008; Ko and Robitaille, 2015; Darabid et al., 2014; Reddy et al., 2003*), PSCs have been shown to guide motor axon innervation and synaptogenesis (*Reddy et al., 2003; Trachtenberg and Thompson, 1997; Koirala et al., 2000; O'Malley et al., 1999; Barik et al., 2016*), support compensatory axonal sprouting (*Astrow et al., 1994; Reynolds and Woolf, 1992; Son and Thompson, 1995; Love and Thompson, 1998*), participate in synaptic pruning (*Griffin and Thompson, 2008; Lee et al., 2017; Smith et al., 2013; Darabid et al., 2013*), and detect and modulate cholinergic transmission (*Ko and Robitaille, 2015; Jahromi et al., 1992; Reist and Smith, 1992; Robitaille, 1995; Robitaille et al., 1997; Rochon et al., 2001*).

While great progress has been made in understanding the cellular and physiological characteristics of PSCs, very little is known about the molecular composition of these cells (*Ko and Robitaille, 2015*). This has been due to the absence of a cell-specific molecular marker with which PSCs can be identified, isolated, and genetically manipulated. This has hindered examinations of the processes of PSC development, differentiation and turnover. Additionally, isolation and targeting of PSCs for interrogation of molecular function in vivo and in vitro has not been possible. Therefore, the discovery of markers specific to PSCs is necessary to advance our understanding of PSCs, and synaptic glia in general, on multiple fronts.

A growing number of molecular markers that recognize subsets of glial cells throughout the nervous system have been identified (*Jäkel and Dimou, 2017*). Therefore, we explored the possibility that a unique combination of glial cell markers could be used to distinguish PSCs. We have found that PSCs can be identified by the combined expression of the calcium-binding protein B (S100 $\beta$ ) (*Brockes et al., 1979; Perez and Moore, 1968*) and neuron-glia antigen-2 (NG2) (*Stallcup, 1981; Bergles et al., 2010*) genes. We utilized this unique molecular fingerprint to create a transgenic mouse that enables visualization and isolation of PSCs in a cell specific manner. This genetic model will help overcome obstacles to understanding the cellular and molecular rules that govern PSC function at NMJs during development, following injury, in old age, and in diseases, such as Amyotrophic Lateral Sclerosis (ALS).

## Results

To identify unique markers for PSCs, we examined the expression of genes shown to be co-expressed with well-established markers of Schwann cells in a subset of glial cells in the central nervous system in PSCs. We focused on NG2 for the following reasons: 1) it has been found to be co-expressed with S100 $\beta$ , a classical marker of all Schwann cells, in a subset of glial cells in the developing brain (*Matthias et al., 2003; Hachem et al., 2005; Vives et al., 2003; Moshrefi-Ravasdjani et al., 2017; Platel et al., 2009*); 2) published data show that it is expressed in skeletal muscles and labels pericytes and neural progenitor cells (*Birbrair et al., 2013a; Birbrair et al., 2013b*). To determine if NG2 is expressed by PSCs, we examined whole-mounted extensor digitorum longus (EDL) muscles from NG2-dsRed mice (*Zhu et al., 2008*). We observed widespread distribution of NG2-dsRed positive cells in the EDL muscle, including a distinct subset of cells located specifically at the NMJ and with a similar morphology as PSCs (*Figure 1C*). To determine if NG2 is expressed in PSCs we generated a transgenic mouse line (referred herein as S100 $\beta$ -GFP;NG2-dsRed; *Figure 1A*) by crossing the NG2-dsRed line with the S100 $\beta$ -GFP mouse line in which the S100 $\beta$  promoter drives expression of GFP in all Schwann cells (*Zuo et al., 2004*). As expected, in the resulting S100 $\beta$ -GFP;NG2-dsRed double transgenic mouse line, dsRed labeled all NG2 positive cells (referred herein as NG2-dsRed<sup>+</sup>) and GFP labeled all Schwann cells (referred herein as S100 $\beta$ -GFP<sup>+</sup>) (*Figure 1B–C*) in skeletal muscles. However, we found a select subset of glia positive for both S100 $\beta$ -GFP and NG2-dsRed specifically located at the NMJ (yellow cells in *Figure 1D*). Based on the location and morphology of the cell body and its elaborations, we concluded that PSCs are the only cells expressing both S100 $\beta$ -GFP and NG2-dsRed in skeletal muscles.

We next evaluated whether the S100 $\beta$ -GFP;NG2-dsRed mouse line serves as a reliable model to study PSCs and their roles at NMJs. In healthy young adult muscle, we observed the same number of PSCs at NMJs in the EDL muscle of S100 $\beta$ -GFP and S100 $\beta$ -GFP;NG2-dsRed mice (*Figure 2A–C*). The morphology of PSCs also appeared to be indistinguishable between the two transgenic lines. In addition, the morphology of NMJs, as assessed by fragmentation of nicotinic acetylcholine receptor

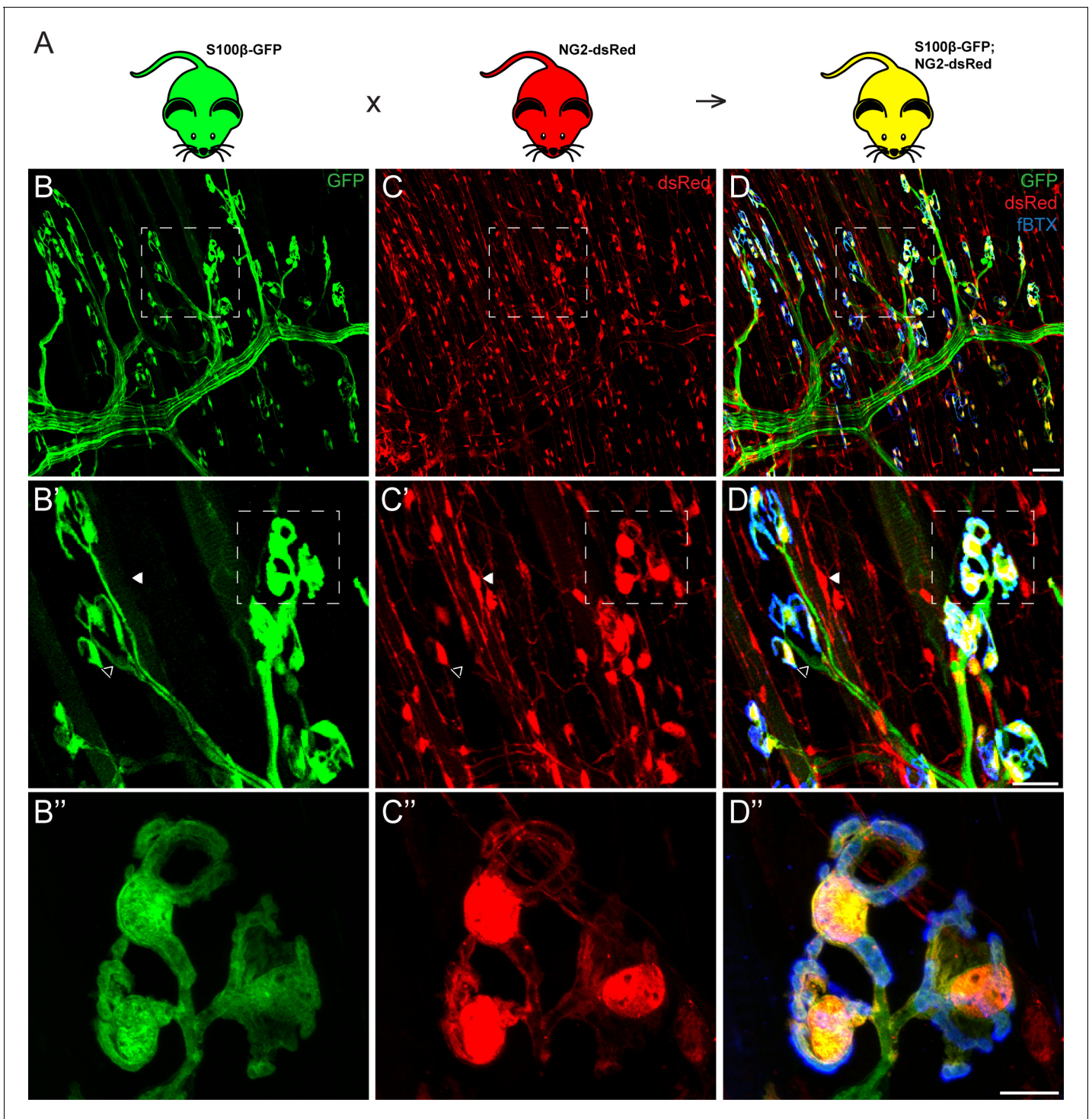


**Figure 1.** Co-expression of S100 $\beta$  and NG2 is unique to PSCs in the EDL muscle. (A) In order to selectively label PSCs, S100 $\beta$ -GFP and NG2-dsRed transgenic mice were crossed to create S100 $\beta$ -GFP;NG2-dsRed mice. (B–D) Representative images of GFP (B) and dsRed (C) fluorescence in the EDL of S100 $\beta$ -GFP;NG2-dsRed mice. S100 $\beta$ -GFP+ Schwann cells are visible along the motor axon while S100 $\beta$ -GFP+ PSCs are identified by their unique morphology and clustering pattern near the NMJ, visualized here using a fluorescent  $\alpha$ -bungarotoxin conjugate (fBTX) to detect nAChRs (blue). Note that PSCs are the only cells expressing both GFP and dsRed (D). At non-synaptic sites, GFP-positive cells do not express dsRed (hollow arrow; B', C', D') and dsRed-positive cells do not express GFP (filled arrow; B', C', D'). Scale bar = 50  $\mu$ m (D), 25  $\mu$ m (D'), and 10  $\mu$ m (D'').

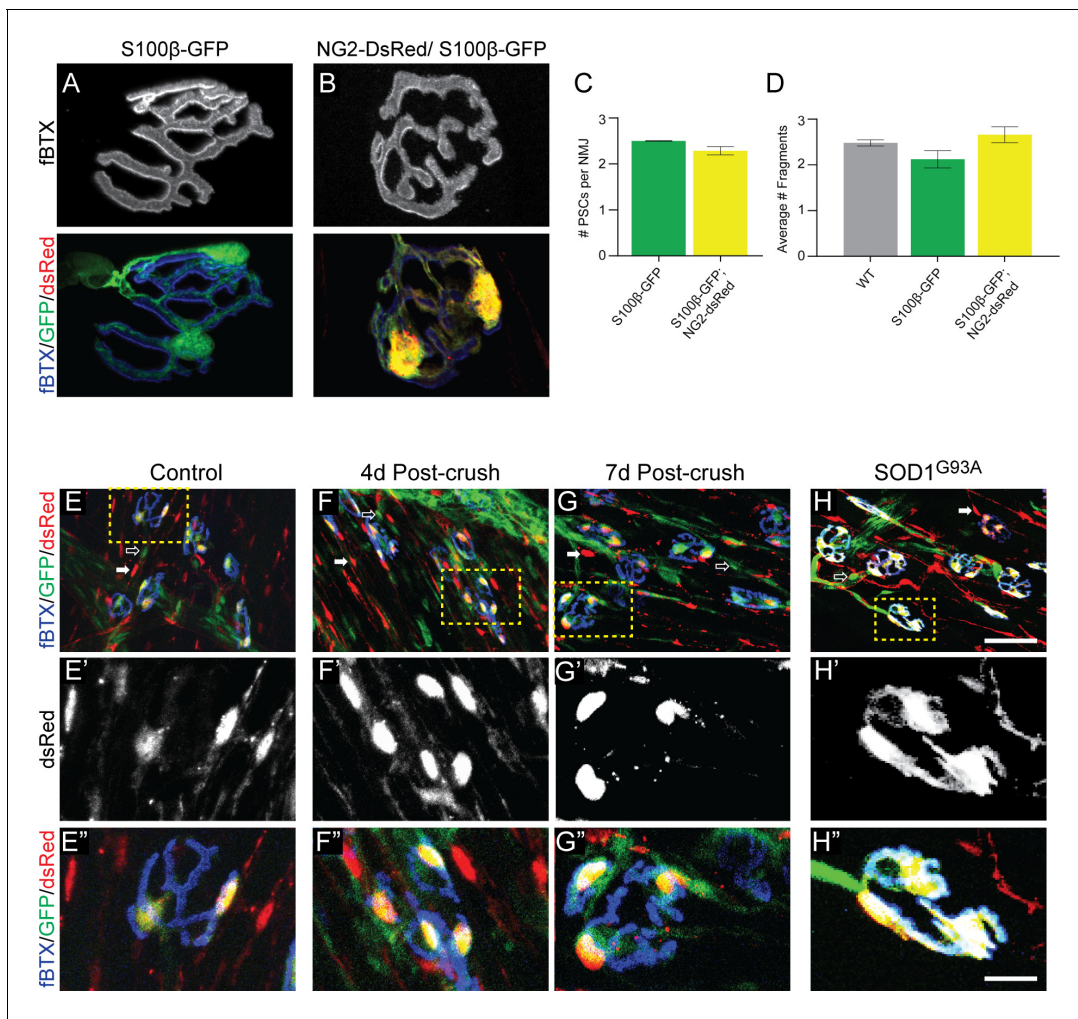


**Figure 2.** The NG2-DsRed/S100 $\beta$ -GFP mouse line can be used to reliably identify PSCs in healthy and stressed NMJs. (A–B) Representative images of NMJs identified by fBTX labeled nAChRs from S100 $\beta$ -GFP (A) and S100 $\beta$ -GFP;NG2-dsRed (B) EDL. (C–D) The co-expression of GFP and dsRed has no discernible negative effects on NMJ fragmentation or PSC number in the EDL muscle of young adult mice. (C) The average number of PSCs per NMJ is unchanged between S100 $\beta$ -GFP mice and S100 $\beta$ -GFP;NG2-dsRed mice. (D) The average number of nAChR fragments per NMJ, as determined by analysis of continuity of fBTX labeled nAChRs, is unchanged between wild-type, S100 $\beta$ -GFP, and S100 $\beta$ -GFP;NG2-dsRed animals. (E–H) PSCs in stressed muscle co-express S100 $\beta$ -GFP and NG2-dsRed. Representative images of NMJs identified by fBTX labeled nAChRs in S100 $\beta$ -GFP;NG2-dsRed mice shows co-expression of S100 $\beta$ -GFP and NG2-dsRed by PSCs in healthy uninjured (E), at 4d (F), and 7d (G) post-fibular nerve crush, and in P120 SOD1G93A (H) EDL. At non-synaptic sites, GFP-positive cells do not express dsRed (hollow arrow; E, F, G, H) and dsRed-positive cells do not express GFP (filled arrow; E, F, G, H). Error bar = standard error of the mean. Scale bar = 10  $\mu$ m (A–B), 50  $\mu$ m (E–H), and 12.5  $\mu$ m (E'–H' and E''=H').

(nAChR) clusters, is unchanged in S100 $\beta$ -GFP;NG2-dsRed mice compared to S100 $\beta$ -GFP and wild type mice (Figure 2A,B,D). Thus, the co-expression of S100 $\beta$ -GFP and NG2-dsRed does not appear to cause apparent deleterious changes on either PSCs or the postsynaptic region revealed by nAChRs. However, it remains possible that co-expression of these markers in PSCs may disrupt the presynapse and biophysical properties of the NMJ. If so, we hypothesize that such changes would be minor given that S100 $\beta$ -GFP;NG2-dsRed mice are outwardly indistinguishable when compared to S100 $\beta$ -GFP and wild type mice.

We next assessed if S100 $\beta$ -GFP;NG2-dsRed mice could also be used to study PSCs at degenerating and regenerating NMJs. First, we examined expression of NG2-dsRed and S100 $\beta$ -GFP after crushing the fibular nerve (Dalkin et al., 2016). In this injury model, motor axons completely retract within 1 day and return to reinnervate vacated postsynaptic sites by 7 days post-injury in young adult mice. Similar to healthy uninjured EDL muscles (Figure 2E), NG2-dsRed and S100 $\beta$ -GFP were found co-expressed exclusively in PSCs at 4d and 7d post-injury (Figure 2F–G). Second, we crossed the

SOD1<sup>G93A</sup> mouse line, (Gurney et al., 1994) a model of ALS shown to exhibit significant degeneration of NMJs (Moloney et al., 2014), with S100β-GFP;NG2-dsRed mice and examined the expression pattern of NG2-dsRed and S100β-GFP in the EDL during the symptomatic stage (P120). We again found NG2-dsRed and S100β-GFP co-expressed only in PSCs in the EDL of P120 SOD1<sup>G93A</sup>; S100β-GFP;NG2-dsRed mice (Figure 2H). Together, these data strongly indicate that this genetic labeling approach can be deployed to study the synaptic glia of the NMJ in a manner previously not possible in healthy and stressed NMJs.

To determine the relationship between NG2 expression and PSC differentiation, we analyzed NG2 expression in S100β-GFP<sup>+</sup> Schwann cells during the course of NMJ development in the EDL muscle of S100β-GFP;NG2-dsRed mice (Figure 3A and Figure 3—figure supplement 1). We observed the presence of S100β-GFP<sup>+</sup> cells at the NMJ as early as embryonic day 15 (E15) with 100% of NMJs having at least one S100β-GFP<sup>+</sup> cell by post-natal day 9 (Figure 3A,B). During the embryonic developmental stages, we observed that NMJs are exclusively populated by S100β-GFP<sup>+</sup>

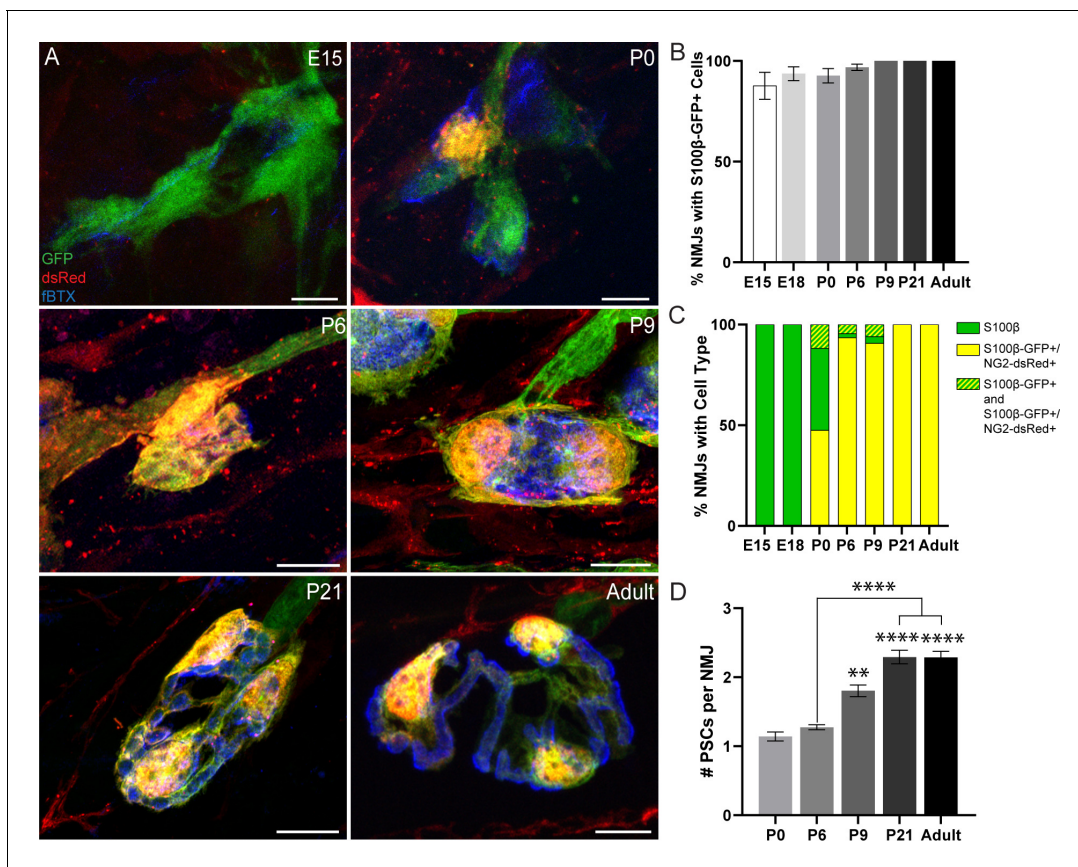


**Figure 3.** Analysis of NG2-dsRed distribution and PSC density during NMJ development in the EDL muscle. (A) Representative images of NMJs, identified by nAChR clusters with fBTX (blue), in developing (E15, P0, P6, P9, P21) and adult S100β-GFP (green);NG2-dsRed (red) transgenic EDL. (B) The number of NMJs populated by at least one S100β-GFP<sup>+</sup> cell increases between the ages of E15 and P9, at which point all observed NMJs have at least one S100β-GFP<sup>+</sup> cell. (C) Analysis of NMJs that contain at least one single labeled S100β-GFP<sup>+</sup> cell (green bar), at least one double labeled S100β-GFP<sup>+</sup>;NG2-dsRed<sup>+</sup> cell (yellow bar) or a combination of single labeled S100β-GFP<sup>+</sup> cells and double labeled S100β-GFP<sup>+</sup>;NG2-dsRed<sup>+</sup> cells (green/yellow bar) shows that developing NMJs are exclusively populated by S100β-GFP<sup>+</sup> cells in the embryonic stages and are increasingly populated by S100β-GFP<sup>+</sup>;NG2-dsRed<sup>+</sup> cells as the NMJ develops. (D) The average number of PSCs per NMJ increases during development. Error bar = standard error of the mean. Scale bar = 10 μm. \*=*p* < 0.05, \*\*=*p* < 0.001, \*\*\*\*=*p* < 0.0001. Asterisks represent comparisons with P0 unless otherwise noted.

The online version of this article includes the following figure supplement(s) for figure 3:

**Figure supplement 1.** Color and grayscale images of PSCs in the EDL muscle of (A) E15, (B) E18, (C) P0, (D) P6, (E) P9, (F) P21, and (G) adult S100β-GFP;NG2-dsRed mice.

**Figure supplement 2.** Cells at NMJs express NG2 in adults but not at embryonic timepoints.

cells that do not express NG2-dsRed (**Figure 3C**). At post-natal day 0 (P0), however, we observed NG2-dsRed expression in a small subset of S100 $\beta$ -GFP<sup>+</sup> cells (**Figure 3A,C**). Notably, the proportion of NMJs with S100 $\beta$ -GFP<sup>+</sup>;NG2-dsRed<sup>+</sup> cells sharply increased between the ages of P0 and P9, coinciding with the period of NMJ maturation in mouse skeletal muscles (**Figure 3C**). By P21, when NMJ maturation in mice is near completion (*Sanes and Lichtman, 1999*), we observed S100 $\beta$ -GFP<sup>+</sup>;NG2-dsRed<sup>+</sup> cells to be exclusively present at NMJs (**Figure 3C**). At this age, the number of S100 $\beta$ -GFP<sup>+</sup>;NG2-dsRed<sup>+</sup> PSCs reached an average of 2.3 per NMJ and this remained unchanged in healthy young adult mice (**Figure 3A,D**). To confirm that dsRed expression from the NG2 promoter denotes the temporal and spatial transcriptional control of the NG2 gene in S100 $\beta$ -GFP;NG2-dsRed mice, we immunostained for NG2 protein. We found NG2 protein present at mature NMJs but not in NMJs of E18 mice with IHC (**Figure 3—figure supplement 2**). Thus, the induced expression of NG2 during the course of NMJ development in Schwann cells located proximally to the NMJ provides further evidence that NG2 is a marker of mature, differentiated S100 $\beta$ <sup>+</sup> PSCs. It is possible that PSCs upregulate NG2 during development in order to restrict motor axon growth at the NMJ (*Filous et al., 2014*). Induced NG2 expression during NMJ development along with the constant presence of S100 $\beta$ -GFP<sup>+</sup> cells (S100 $\beta$ -GFP<sup>+</sup> or S100 $\beta$ -GFP<sup>+</sup>;NG2-dsRed<sup>+</sup>) and absence of single labeled NG2-dsRed<sup>+</sup> cells at NMJs at every observed developmental time point (**Figure 3B,C**) strongly support previous studies indicating that PSCs originate from Schwann cells (*Lee et al., 2017*).

To gain insights into the rules that govern the distribution of PSCs at NMJs we compared PSC density in EDL, soleus, and diaphragm muscles to determine if PSC density is similar across muscles with varying NMJ sizes, fiber types and functional demands. Here, we observed similar PSC densities in each muscle type (**Figure 4—figure supplement 1**), suggesting that the number of PSCs directly correlates with the size of the NMJ and not the functional characteristics or fiber type composition of the muscles with which they are associated.

We next examined the spatial distribution of PSCs at the NMJ using the Nearest Neighbor (NN) analysis. This analysis measures the linear distance between neighboring cells in order to determine the regularity of spacing (*Wassle and Riemann, 1978; Cook, 1996*), quantified using the regularity index. In this analysis, randomly distributed groups of cells yield a nearest neighbor regularity index (NNRI) of 1.91 while those with nonrandom, regularly ordered distributions yield higher NNRI values (*Reese and Keeley, 2015; Figure 4A*). We found that the spacing of PSCs yielded high NNRI values and thus maintained ordered, non-random distributions at NMJs in the EDL muscle of adult mice. Moreover, this ordered distribution was maintained regardless of the overall number of PSCs at a given NMJ (**Figure 4B–D**). These observations are in accord with a published study indicating that PSCs occupy distinct territories at adult NMJs (*Brill et al., 2011*). In addition, these data strongly suggest that presynaptic, postsynaptic, and/or PSC-PSC mechanisms of communication dictate the spatial distribution of PSCs.

The ability to distinguish PSCs from all other Schwann cells makes it possible to identify genes that are either preferentially or specifically expressed in PSCs. We deployed fluorescence-activated cell sorting (FACS) to separately isolate double labeled S100 $\beta$ -GFP<sup>+</sup>;NG2-dsRed<sup>+</sup> PSCs, single-labeled S100 $\beta$ -GFP<sup>+</sup> Schwann cells, and single-labeled NG2-dsRed<sup>+</sup> cells (including  $\alpha$ -SMA pericytes and Tuj1<sup>+</sup> precursor cells [*Birbrair et al., 2013b*]) from juvenile (P15–P22) S100 $\beta$ -GFP;NG2-dsRed transgenic mice. We then utilized RNA-Sequencing (RNA Seq) to compare the transcriptional profile of PSCs with the other two groups (**Figure 5A**). Light microscopy and expression analysis of GFP and dsRed using quantitative PCR (qPCR) confirmed that only cells of interest were sorted (**Figure 5A–B**). This analysis revealed a unique transcriptional profile for PSCs (**Figure 5C**). Notably, we found 567 genes enriched in PSCs that were not previously recognized to be associated with PSCs, glial cells or synapses (**Supplementary file 1**) using Ingenuity Pathway Analysis (IPA). We also found a number of genes preferentially expressed by PSCs with known roles at synapses (*Mozer and Sandstrom, 2012; Fox and Umemori, 2006; Rafuse et al., 2000; Ranaivoson et al., 2019; Shapiro et al., 2007; Peng et al., 2010; Supplementary file 1*). Providing additional insights about the function of PSCs, IPA revealed synaptogenesis, glutamate receptor, and axon guidance signaling as top canonical pathways under transcriptional regulation (**Figure 5D**).

We next cross-referenced our transcriptomic data with a list of genes compiled from published studies indicating enrichment or functional roles in PSCs (*Young et al., 2005; Reynolds and Woolf, 1992; Robitaille, 1995; Robitaille et al., 1997; Rochon et al., 2001; Georgiou and Charlton, 1999; Trachtenberg and Thompson, 1996; Morris et al., 1999; Woldeyesus et al., 1999;*

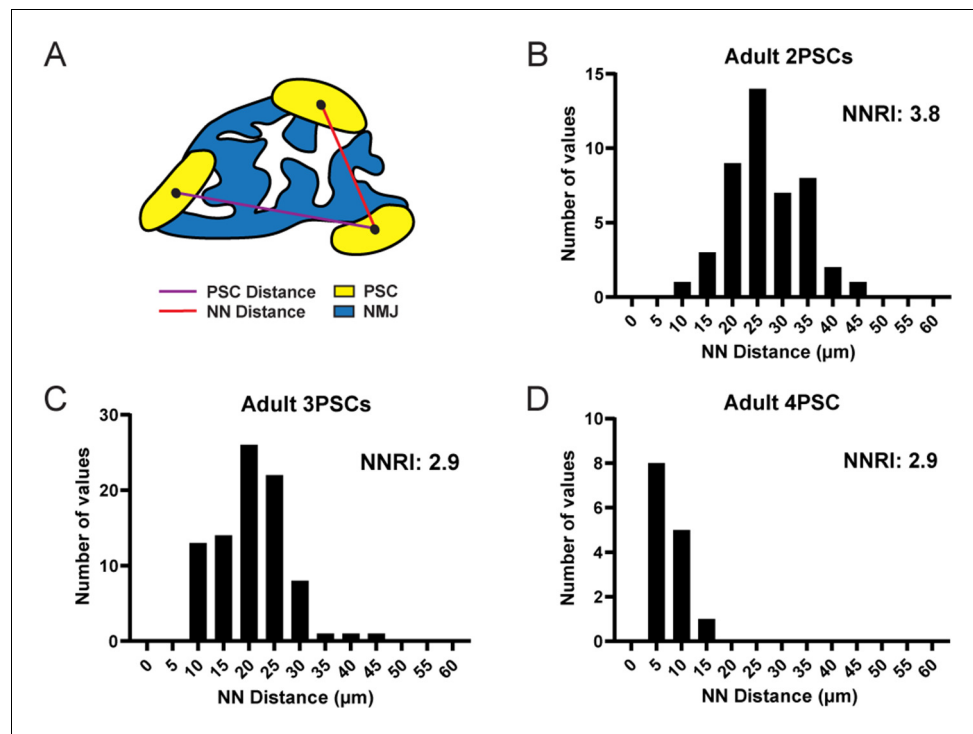


**Figure 4.** PSC distribution at the NMJ is non-random and ordered. (A) The nearest neighbor (NN) distance, or the distance between a PSC and the closest neighboring PSC, is represented by the red line. The distance represented by the purple line is not considered for NN analysis. The distribution of NN values (shown in panels B, C, and D) is used to determine the degree of order in PSC distribution, as represented by the nearest neighbor regularity index (NNRI). Distribution patterns with an NNRI value greater than 1.91 are considered to be non-random. (B–D) Nearest neighbor distributions of S100-GFP+;NG2-dsRed+ PSCs in adult (P60) EDL muscle show that PSC distributions have orderly patterns of distribution with NNRI > 1.91 regardless of whether they are located at an NMJ with 2 PSCs (B), 3 PSCs (C), or 4 PSCs (D).

The online version of this article includes the following figure supplement(s) for figure 4:

**Figure supplement 1.** The number of PSCs associated with an NMJ varies but PSC density remains constant in the EDL, soleus (SOL), and diaphragm (DIA) muscles of adult mice.

Riethmacher et al., 1997; Personius et al., 2016; Park et al., 2017; Pinard et al., 2003; Descarries et al., 1998; Hess et al., 2007; Heredia et al., 2018; Darabid et al., 2018; Musarella et al., 2006; De Winter et al., 2006; Feng and Ko, 2008; Yang et al., 2001; Petrov et al., 2014; Robitaille et al., 1996; Gorlewicz et al., 2009; Wright et al., 2009). This analysis identified 27 genes expressed in isolated S100β-GFP+;NG2-dsRed+ PSCs that were previously shown to be associated with PSCs (Table 1). These included genes involved in detection and modulation of synaptic activity such as adenosine (Robitaille, 1995; Rochon et al., 2001), P2Y (Robitaille, 1995; Heredia et al., 2018; Darabid et al., 2018), acetylcholine (Robitaille et al., 1997; Petrov et al., 2014; Wright et al., 2009) and glutamate receptors (Pinard et al., 2003), Butyrylcholinesterase (BChE) (Petrov et al., 2014), and L-type calcium channels (Robitaille et al., 1996). Additionally, genes involved in NMJ development, synaptic pruning, and maintenance including agrin, 2',3'-cyclic nucleotide 3' phosphodiesterase (CNP) (Georgiou and Charlton, 1999), Erb-b2 receptor tyrosine kinase 2 (Erb-b2) (Trachtenberg and Thompson, 1996; Morris et al., 1999; Woldeyesus et al., 1999), Erb-b3 (Trachtenberg and Thompson, 1996; Riethmacher et al., 1997) GRB2-associated protein 1 (Gab1) (Park et al., 2017), myelin-associated glycoprotein (MAG) (Georgiou and Charlton, 1999), and myelin protein zero (Mpz) (Georgiou and Charlton, 1999) were detected in PSCs.

We deployed quantitative PCR (qPCR) to validate preferential expression of select genes in PSCs. To do so, we obtained RNA from S100β-GFP+;NG2-dsRed+ PSCs, single-labeled S100β-GFP+

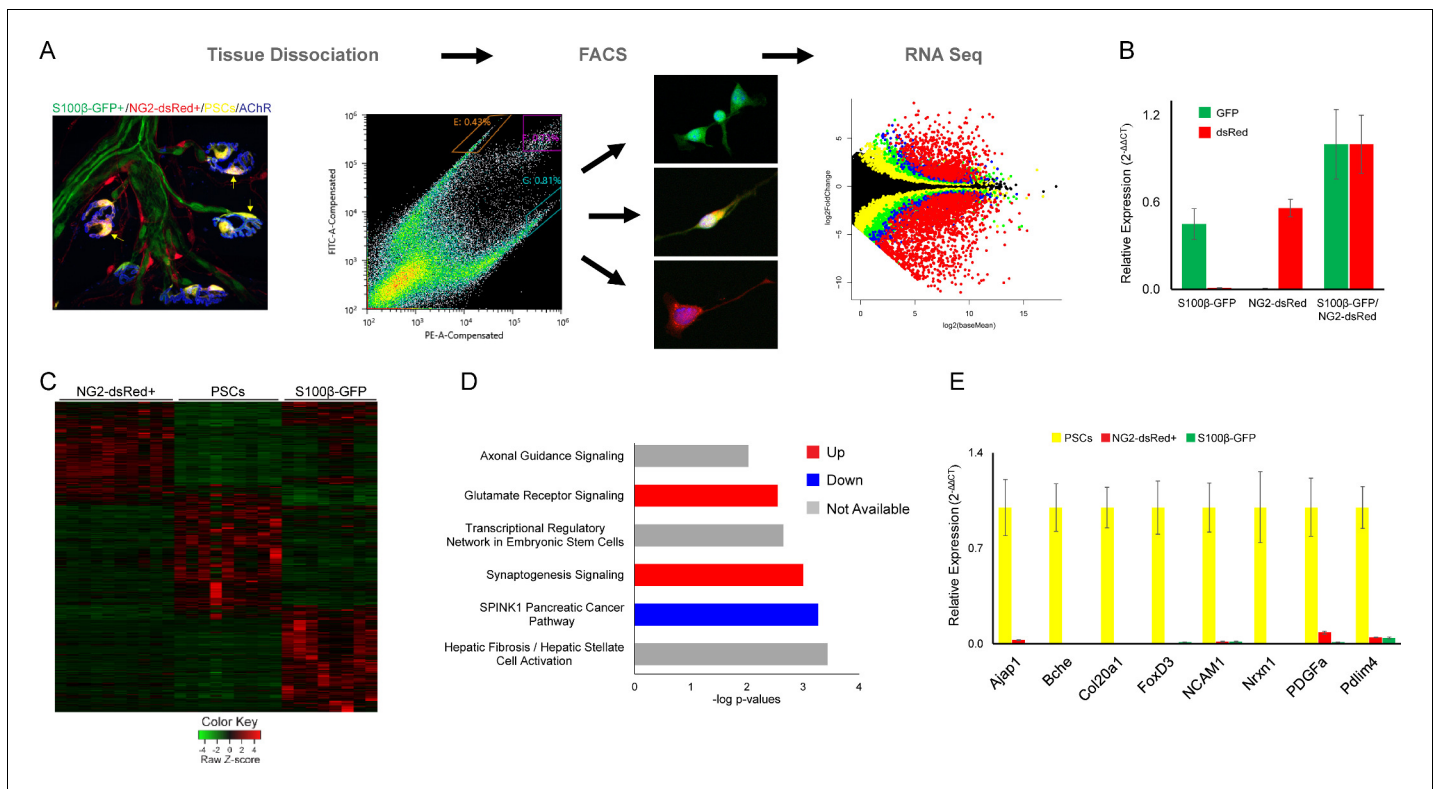


**Figure 5.** Molecular analysis of S100 $\beta$ -GFP $^{+}$ ;NG2-dsRed $^{+}$  PSCs, S100 $\beta$ -GFP $^{+}$  Schwann cells, and NG2-dsRed $^{+}$  cells following isolation with FACS. (A) Skeletal muscle from juvenile S100 $\beta$ -GFP;NG2-dsRed mice was dissociated and S100-GFP $^{+}$ ;NG2-dsRed $^{+}$  PSCs, S100 $\beta$ -GFP $^{+}$  Schwann cells, and NG2-dsRed $^{+}$  cells were sorted by FACS for RNA seq and qPCR. Representative fluorescence intensity gates for sorting of S100 $\beta$ -GFP $^{+}$ , NG2-dsRed $^{+}$  and S100 $\beta$ -GFP $^{+}$ ;NG2-dsRed $^{+}$  cells are indicated in the scatter plot. GFP (y-axis) and dsRed (x-axis) fluorescence intensities were used to select gates for S100 $\beta$ -GFP $^{+}$  cells (outlined in orange), NG2-dsRed $^{+}$  cells (outlined in teal), and double labeled S100 $\beta$ -GFP $^{+}$ ;NG2-dsRed $^{+}$  cells (outlined in purple). Representative images of cells from sorted populations are shown. (B) GFP and dsRed qPCR was performed on FACS isolated cells to confirm specificity of sorting gates. (C) A heat map of RNA-seq results depicting genes with at least 5 counts and expression differences with a p-value of less than 0.01 between any 2 cell types reveals a distinct transcriptome in S100 $\beta$ -GFP $^{+}$ ;NG2-dsRed $^{+}$  PSCs versus S100 $\beta$ -GFP $^{+}$  Schwann cells and NG2-dsRed $^{+}$  cells. (D) Synaptogenesis and axon guidance signaling are among the most influential signaling pathways in PSCs according to Ingenuity Pathway Analysis of genes enriched in PSCs versus S100 $\beta$ -GFP $^{+}$ , and NG2-dsRed $^{+}$  cells. (E) qPCR was performed on FACS isolated S100-GFP $^{+}$ ;NG2-dsRed $^{+}$  PSCs, S100 $\beta$ -GFP $^{+}$  Schwann cells, and NG2-dsRed $^{+}$  cells to verify mRNA levels of RNA seq identified PSC enriched genes. In each analysis, transcripts were not detected or detected at low levels in S100 $\beta$ -GFP $^{+}$  Schwann cells and NG2-dsRed $^{+}$  cells. Error bar = standard error of the mean. Scale bar = 10  $\mu$ m.

Schwann cells, and single-labeled NG2-dsRed $^{+}$  cells isolated using FACS from juvenile S100 $\beta$ -GFP;NG2-dsRed transgenic mice. We examined eight genes identified by RNA seq as being highly enriched in PSCs. This included newly identified genes (Ajap1, Col20a1, FoxD3, Nrnx1, PDGFa, and Pdlim4) and genes previously shown to be enriched (BChE [Petrov *et al.*, 2014] and NCAM1 [Covault and Sanes, 1986]) in PSCs (Figure 5E). Validating RNA-Seq findings, qPCR analysis showed that all eight genes are highly enriched in PSCs compared to all other cell types isolated via FACS (Figure 5E). Additionally, immunostaining showed that NG2, a novel PSC-enriched gene identified by RNA-Seq, is concentrated at the NMJ (Figure 3—figure supplement 2).

## Discussion

We have discovered a unique combination of molecular markers that allows us to specifically visualize, isolate, interrogate the transcriptome, and potentially alter the molecular composition of PSCs. We have shown that NG2 is specifically expressed by S100 $\beta$ -GFP $^{+}$  PSCs but not myelinating S100 $\beta$ -GFP $^{+}$  Schwann cells and thus the combined expression of S100 $\beta$  and NG2 is a unique molecular marker of PSCs in skeletal muscle. Providing further evidence that NG2 is a marker of differentiated PSCs, we have demonstrated that Schwann cells induce expression of NG2 shortly after they arrive



**Table 1.** Genes with functional roles in PSCs identified by RNA seq analysis of isolated PSCs.

Gene	Description	Proposed role	Read count	Log2 change vs NG2-dsRed+	Log2 change vs S100β-GFP+	Reference
Adora2a	Adenosine A2a receptor	Detect/modulate synaptic activity	8.1	-3.68	-2.67	(Robitaille, 1995; Rochon et al., 2001)
Adora2b	Adenosine A2b receptor	Detect/modulate synaptic activity	9.2	-3.16	-4.55	(Robitaille, 1995; Rochon et al., 2001)
Agrn	Agrin	AChR aggregation	2049.7	1.16	2.93	(Georgiou and Charlton, 1999)
Bche	Butyrylcholinesterase	Modulate synaptic ACh levels	7191.0	7.89	7.21	(Trachtenberg and Thompson, 1996)
Cacna1c	L type Calcium channel, alpha 1 c	Detect/modulate synaptic activity	14.3	-4.92	-2.10	(Morris et al., 1999)
Cacna1d	L type Calcium channel, alpha 1d	Detect/modulate synaptic activity	18.4	-0.42	-1.49	(Morris et al., 1999)
Cd44	CD44 antigen	Mediates cell-cell interactions	1249.2	0.75	-1.22	(Woldeyesus et al., 1999)
Chrm1	Muscarinic acetylcholine receptor M1	Detect/modulate synaptic activity	14.8	n.d.	0.89	(Robitaille et al., 1997; Riethmacher et al., 1997)
Cnp	2',3'-cyclicnucleotide 3' phosphodiesterase	Anchors axon terminal at NMJ	2990.2	4.23	1.66	(Personius et al., 2016)
ErbB2	Erb-b2 receptor tyrosine kinase 2	Synaptogenesis/maintenance	228.9	0.84	1.37	(Park et al., 2017; Pinard et al., 2003; Descarries et al., 1998)
ErbB3	Erb-b2 receptor tyrosine kinase 3	Synaptogenesis/maintenance	2471.3	7.05	4.46	(Park et al., 2017; Hess et al., 2007)
GAb1	GRB2-associated protein 1	Synaptic pruning	693.8	0.31	1.57	(Heredia et al., 2018)
Grm1	Glutamate receptor, metabotropic 1	Detect/modulate synaptic activity	9.2	n.d.	0.80	(Darabid et al., 2018)
Grm5	Glutamate receptor, metabotropic 5	Detect/modulate synaptic activity	38.0	n.d.	2.84	(Darabid et al., 2018)
LNx1	Ligand of numb-protein X 1	Regulate NRG1 signaling	37.5	-2.29	-0.70	(Peper et al., 1974)
MAG	Myelin-associated glycoprotein	Synaptogenesis/maintenance	136.0	3.12	-0.55	(Personius et al., 2016)
Mpz	Myelin protein zero	Synaptogenesis/maintenance	4590.7	2.54	-0.79	(Personius et al., 2016)
Nos2	Nitric oxide synthase 2, inducible	Synaptogenesis/modulate synaptic activity	13.4	-2.91	-1.28	(Musarella et al., 2006)
Nos3	Nitric oxide synthase 3, endothelial cell	Synaptogenesis/modulate synaptic activity	48.6	-2.69	-0.68	(Musarella et al., 2006)
P2ry1	Purinergic receptor P2Y1	Detect/modulate synaptic activity, synapse elimination	144.4	0.52	2.21	(Robitaille, 1995; De Winter et al., 2006; Feng and Ko, 2008)
P2ry2	Purinergic receptor P2Y2	Detect/modulate synaptic activity	24.0	-1.55	-1.04	(Robitaille, 1995)
P2ry10b	P2Y receptor family member P2Y10b	Detect/modulate synaptic activity	10.0	-1.25	-3.14	(Robitaille, 1995)
P2ry12	P2Y receptor family member P2Y12	Detect/modulate synaptic activity	273.5	n.d.	3.70	(Robitaille, 1995)
P2ry14	P2Y receptor family member P2Y14	Detect/modulate synaptic activity	13.6	-3.49	-2.06	(Robitaille, 1995)
S100b	S100 protein beta	Intracellular signaling	1788.3	5.34	3.12	(Reynolds and Woolf, 1992)
Sema3a	Semaphorin 3a	Detect/modulate synaptic activity	136.6	2.95	1.07	(Yang et al., 2001)
Tgfb1	Transforming growth factor, beta 1	AChR aggregation	173.2	-1.08	-1.90	(Petrov et al., 2014)

at the NMJ during maturation of the synapse. However, the means by which the induced expression of NG2 is part of a program to establish and/or further specify PSC identity in Schwann cells at the NMJ, through activation of the NG2 promoter, remains to be determined.

We utilized FACS to isolate S100 $\beta$ -GFP<sup>+</sup>;NG2-dsRed<sup>+</sup> PSCs from skeletal muscle to analyze the PSC transcriptome. To our knowledge this is the first time that the transcriptome of PSCs, or any other type of glial cell that associates exclusively with synapses, has been characterized. This analysis reveals expression of a number of genes that have been previously implicated in modulation of synaptic activity, synaptic pruning, and synaptic maintenance by PSCs. We identified a number of novel genes that are highly expressed in PSCs but not Schwann cells or NG2<sup>+</sup> cells. These genes have the potential to assist PSC research by serving as molecular markers that can be utilized for PSC-specific genetic manipulations, PSC ablation, and isolation of PSCs for cell culture and molecular analysis. We verified a number of these with qPCR and IHC. This analysis, therefore, reveals a unique gene expression signature that distinguishes PSCs from all other Schwann cells.

While the role of the majority of genes found enriched in PSCs at the neuromuscular synapse remains to be determined, it is worth noting that many have been shown to play key roles in neuronal circuits in the central nervous system and in cell-cell communication. This is the case for NG2 which has been shown to terminate axonal growth in glial scars in the spinal cord (Filous *et al.*, 2014). Therefore, it is possible that NG2 is utilized by PSCs to tile, and thus occupy unique territories, and prevent motor axons from developing sprouts that extend beyond the postsynaptic partner. Supporting this possibility, we have found that the NG2 promoter is active in some PSCs at P0 (Figure 3C), a time when motor axon nerve endings at NMJs undergo rapid morphological changes (Sanes and Lichtman, 1999; Sanes and Lichtman, 2001). The progressive activation of the NG2 promoter in PSCs is complete by P9 (Figure 3C), which coincides with the elimination of extraneuronal axons innervating the same postsynaptic site in mice (Sanes and Lichtman, 1999; Sanes and Lichtman, 2001). Therefore, PSCs may utilize NG2 to promote the maturation of the presynaptic region and thus the NMJ. Furthermore, PSCs may utilize NG2 to repel each other as they tile during development to occupy unique territories at the NMJ (Brill *et al.*, 2011).

With these tools, it is now possible to determine which cellular and molecular determinants are critical for PSC differentiation, maturation, and function at the NMJ. It will also allow us to ascertain the contribution of PSCs to NMJ repair following injury and NMJ degeneration during normal aging and the progression of neuromuscular diseases, such as Amyotrophic Lateral Sclerosis (ALS) and Spinal Muscular Atrophy (SMA). Our strategy of specifically labeling synaptic glia, using a combination of protein markers uniquely expressed in this cell type, may serve as a springboard for unprecedented approaches for studying not only PSC function at the NMJ, but also synapse-associated glia throughout the CNS. Indeed, we have observed subsets of astrocytes in the brain that co-express both S100 $\beta$  and NG2, as has been previously reported in the context of a lineage tracing analysis (Deloulme *et al.*, 2004). Future studies will determine the generality of our approach in discerning the functional roles of synaptic glia in the development, maintenance, and function of select synapses.

## Materials and methods

### Key resources table

Reagent type (species) or resource	Designation	Source or reference	Identifiers	Additional information
Genetic reagent ( <i>M. musculus</i> )	S100b-GFP	PMID:15590915	MGI:3588512	Dr. Wesley Thompson (Texas A and M)
Genetic reagent ( <i>M. musculus</i> )	NG2-dsRed	PMID:18045844	MGI:3796063	Dr. Akiko Nishiyama (University of Connecticut)
Genetic reagent ( <i>M. musculus</i> )	SOD1 <sup>G93A</sup>	PMID:8209258	MGI:2183719	Dr. Deng (Northwestern University)

Continued on next page

Continued

Reagent type (species) or resource	Designation	Source or reference	Identifiers	Additional information
Antibody	Guinea pig polyclonal anti-NG2	PMID: <a href="#">19058188</a>	Antibody Registry: AB_2572299	1:250
Antibody	Alexa Fluor-488 goat polyclonal anti guinea pig	Invitrogen	RRID: <a href="#">AB_2534117</a>	1:1000
Antibody	Alexa Fluor-488 goat polyclonal anti rabbit	Invitrogen	Catalog# A-11008	1:1000
Software, algorithm	Ingenuity Pathway Analysis	Qiagen	RRID: <a href="#">SCR_008117</a>	
Software, algorithm	GraphPad Prism	GraphPad	RRID: <a href="#">SCR_002798</a>	
Software, algorithm	R	The R Project for Statistical Computing	RRID: <a href="#">SCR_001905</a>	
Software, algorithm	ImageJ	ImageJ	RRID: <a href="#">SCR_003070</a>	
Software, algorithm	Bio-Rad CFX Manager	Bio-Rad	RRID: <a href="#">SCR_017251</a>	
Commercial assay or kit	PicoPure RNA Isolation Kit	ThermoFisher	Catalog#KIT0204	
Commercial assay or kit	iScript cDNA synthesis kit	Bio-Rad	Catalog#1708891	
Commercial assay or kit	SsoAdvanced PreAmp Supermix	Bio-Rad	Catalog#1725160	
Commercial assay or kit	iTAQ Universal SYBR Green Supermix	Bio-Rad	Catalog#1725121	
Chemical compound, drug	Alexa Fluor-555 alpha-bungarotoxin	Invitrogen	Catalog#B35451	
Chemical compound, drug	DAPI	ThermoFisher	Catalog#D1306	

## Mice

SOD1<sup>G93A98</sup> (Gurney et al., 1994), S100 $\beta$ -GFP (B6;D2-Tg(S100b-EGFP)1Wjt/J) (Zuo et al., 2004) and NG2-dsRed mice (Tg(Cspg4-DsRed.T1)1Akik/J) (Zhu et al., 2008) were obtained from Jackson Labs (Bar Harbor, ME). S100 $\beta$ -GFP and NG2-dsRed mice were crossed to generate S100 $\beta$ -GFP;NG2-dsRed mice. Offspring were genotyped using Zeiss LSM900 to check for fluorescent labels. SOD1<sup>G93A</sup> mice were crossed with S100 $\beta$ -GFP;NG2-dsRed mice to generate S100 $\beta$ -GFP;NG2-dsRed;SOD1<sup>G93A</sup> mice. Postnatal mice older than 9 days of age were anesthetized and immediately perfused with 4% paraformaldehyde (PFA) overnight. Pups were anesthetized by isoflurane and euthanized by cervical dislocation prior to muscle dissociation. Adult mice were anesthetized using CO<sub>2</sub> and then perfused transcardially with 10 ml of 0.1 M PBS, followed by 25 ml of ice-cold 4% PFA in 0.1 M PBS (pH 7.4). All experiments were carried out under NIH guidelines and animal protocols approved by the Brown University and Virginia Tech Institutional Animal Care and Use Committee.

## Fibular nerve crush

Adult S100 $\beta$ -GFP;NG2-dsRed mice were anesthetized with a mixture of ketamine (100 mg/kg) and xylazine (10 mg/kg) delivered intraperitoneally. The fibular nerve was crushed at its intersection with

the lateral tendon of the gastrocnemius muscle using fine forceps, as described previously (Dalkin *et al.*, 2016). Mice were monitored for 2 hr following surgery and administered buprenorphine (0.05–0.10 mg/kg) at 12 hr intervals during recovery.

### Immunohistochemistry and NMJ visualization

For NG2 immunohistochemistry (IHC), muscles were incubated in blocking buffer (5% lamb serum, 3% BSA, 0.5% Triton X-100 in PBS) at room temperature for 2 hr, incubated with anti-NG2 antibody (courtesy of Dr. Dwight Bergles) diluted at 1:250 in blocking buffer overnight at 4°C, washed 3 times with 0.1M PBS for 5 min. Muscles were then incubated with 1:1000 Alexa Fluor-488 conjugated anti-rabbit or guinea pig antibody (A-11008, Invitrogen, Carlsbad, CA) and 1:1000 Alexa Fluor-555 conjugated  $\alpha$ -bungarotoxin (fBTX; Invitrogen, B35451) in blocking buffer for 2 hr at room temperature and washed 3 times with 0.1M PBS for 5 min. For all other NMJ visualization, muscles were incubated in Alexa Fluor-647 conjugated  $\alpha$ -bungarotoxin (fBTX; Invitrogen, B35450) at 1:1000 and 4',6-Diamidino-2-Phenylindole, Dihydrochloride (DAPI; D1306, ThermoFisher, Waltham, MA) at 1:1000 in 0.1M PBS at 4°C overnight. Muscles were then washed with 0.1M PBS 3 times for 5 min each. Muscles were whole mounted using Vectashield (H-1000, Vector Labs, Burlingame, CA) and 24 × 50–10.5 cover glass (ThermoFisher).

### Confocal microscopy of PSCs and NMJs

All images were taken with a Zeiss LSM700, Zeiss LSM 710, or Zeiss LSM 900 confocal light microscope (Carl Zeiss, Jena, Germany) with a 20 × air objective (0.8 numerical aperture), 40 × oil immersion objective (1.3 numerical aperture), or 63 × oil immersion objective (1.4 numerical aperture) using the Zeiss Zen Black software. Optical slices within the z-stack were taken at 1.00  $\mu$ m or 2.00  $\mu$ m intervals. High resolution images were acquired using the Zeiss LSM 900 with Airyscan under the 63 × oil immersion objective in super resolution mode. Optical slices within the z-stack were 0.13  $\mu$ m with a frame size of 2210 × 2210 pixels. Images were collapsed into a two-dimensional maximum intensity projection for analysis.

### Image analysis

#### NMJ size

To quantify the area of NMJs, the area of the region occupied by nicotinic acetylcholine receptors (nAChRs, labeled by fBTX, was measured using ImageJ software. At least 100 nAChRs were analyzed for number of fragments, individual nicotinic acetylcholine receptor (nAChR) clusters, from each muscle to represent an individual mouse. At least 3 animals per age group were analyzed to generate the represented data.

#### Cells associated with NMJs

Cell bodies were visualized via GFP and/or dsRed signal, and were confirmed as cell bodies by the presence of a DAPI+ nucleus. The area of each cell body was measured by tracing the outline of the entire cell body using the freehand tool in ImageJ. To quantify the number of cells associated with NMJs, the number of cell bodies directly adjacent to each NMJ was counted. Every cell that overlapped with or directly abutted the fBTX signal was considered adjacent to the NMJ. At least 3 animals per age group were analyzed to generate the represented data. Cells were examined in at least 100 NMJs from each muscle to represent an individual mouse.

#### Spacing of PSCs at NMJs

NMJs were identified via fBTX signal. PSCs were identified by the colocalization of GFP, dsRed, and DAPI signal in addition to their location at NMJs. The area of each PSC and NMJ was measured. The linear distance from the center of each PSC soma to the center of the nearest PSC soma at a single NMJ was measured. The distances were then separated into 5  $\mu$ m bins and plotted in a histogram. All linear measurements were made using the line tool in the ImageJ software. At least 100 NMJs were analyzed from each muscle to represent an individual mouse.

## Muscle dissociation and fluorescence activated cell sorting

Diaphragm, pectoralis, forelimb and hindlimb muscles were collected from P15-P21 S100 $\beta$ -GFP; NG2-dsRed mice. After removal of connective tissue and fat, muscles were cut into 5 mm<sup>2</sup> pieces with forceps and digested in 2 mg/mL collagenase II (Worthington Chemicals, Lakewood, NJ) for 1 hr at 37°C. Muscles were further dissociated by mechanical trituration in Dulbecco's modified eagle medium (Life Technologies, Carlsbad, CA) containing 10% horse serum (Life Technologies) and passed through a 40  $\mu$ m filter to generate a single cell suspension. Excess debris was removed from the suspension by centrifugation in 4% BSA followed by a second centrifugation in 40% Optiprep solution (Sigma-Aldrich, St. Louis, MO) from which the interphase was collected. Cells were diluted in FACS buffer containing 1 mM EDTA, 25 mM Hepes, 1% heat inactivated fetal bovine serum (Life Technologies), in Ca<sup>2+</sup>/Mg<sup>2+</sup> free 1X Dulbecco's phosphate buffered saline (Life Technologies). FACS was performed with a Sony SH800 Cell Sorter (Sony Biotechnology, San Jose, CA). Representative fluorescence intensity gates for sorting of S100-GFP<sup>+</sup>, NG2-dsRed<sup>+</sup> and S100-GFP<sup>+</sup>;NG2-dsRed<sup>+</sup> cells are provided in **Figure 5**. Purity of the sorted cell population was confirmed by visual inspection of sorted cells using an epifluorescence microscope and with dsRed and GFP qPCR (**Figure 5A,B**). A single mouse was used for each replicate and an average of 7500 cells per replicate were collected for each cell group.

## RNA-seq and qPCR

RNA was isolated from S100 $\beta$ -GFP<sup>+</sup>, NG2-dsRed<sup>+</sup>, or S100 $\beta$ -GFP<sup>+</sup>/NG2-dsRed<sup>+</sup> cells following FACS with the PicoPure RNA Isolation Kit (ThermoFisher). The maximum number of cells that could be collected by FACS following dissociation of muscles collected from one mouse was used as a single replicate. On average, a single replicate consisted of 7,500 cells. RNA seq was performed by Genewiz on 12 replicates per cell type. Following sequencing, data were trimmed for both adaptor and quality using a combination of ea-utils and Btrim (Aronesty, 2013; Kong, 2011). Sequencing reads were aligned to the genome using HiSat2 (Kim et al., 2019) and counted via HTSeq (Anders et al., 2015). QC summary statistics were examined to identify any problematic samples (e.g. total read counts, quality and base composition profiles (+/- trimming)), raw fastq formatted data files, aligned files (bam and text file containing sample alignment statistics), and count files (HTSeq text files). Following successful alignment, mRNA differential expression were determined using contrasts of and tested for significance using the Benjamini-Hochberg corrected Wald Test in the R-package DESeq2 (Love et al., 2014). Failed samples were identified by visual inspection of pairs plots and removed from further analysis resulting in the following number of replicates for each cell type: NG2-dsRed<sup>+</sup>, 10; S100 $\beta$ -GFP<sup>+</sup>, 7; NG2-dsRed<sup>+</sup>;S100 $\beta$ -GFP<sup>+</sup>, 9. Functional and pathway analysis was performed using Ingenuity Pathway Analysis (QIAGEN Inc, <https://www.qiagenbioinformatics.com/products/ingenuity-pathway-analysis>). Confirmation of expression of genes identified by RNA-seq was performed on 6 additional replicates of each cell type using quantitative reverse transcriptase PCR (qPCR). Reverse transcription was performed with iScript (Bio-Rad, Hercules, CA) and was followed by a preamplification PCR step with SsoAdvanced PreAmp Supermix (Bio-Rad) prior to qPCR using iTAQ SYBR Green and a CFX Connect Real Time PCR System (Bio-Rad). Relative expression was normalized to 18S using the 2<sup>- $\Delta\Delta$ CT</sup> method. The primers used for both preamplification and qPCR are listed in **Supplementary file 2**.

## Statistics

An unpaired t-test or one-way ANOVA with Bonferroni post hoc analysis were used for statistical evaluation. Data are expressed as the mean  $\pm$  standard error of the mean, and  $p < 0.05$  was considered statistically significant. The number of replicates is as follows: RNA seq, 7–10; qPCR, 6; comparisons between EDL, soleus, and diaphragm, 1; comparison between SOD1<sup>G93A</sup> and healthy adult muscle, 1; all other analyses, 3. Statistical analyses were performed using GraphPad Prism8 and R. Data values and p-values are reported within the text.

## Acknowledgements

We thank members of the Valdez laboratory for providing helpful comments throughout the course of this project.

## Additional information

### Funding

Funder	Grant reference number	Author
National Institutes of Health	R01AG055545	Gregorio Valdez
National Institutes of Health	R56AG051501	Gregorio Valdez
National Institutes of Health	R21NS106313	Gregorio Valdez

The funders had no role in study design, data collection and interpretation, or the decision to submit the work for publication.

### Author contributions

Ryan Castro, Thomas Taetzsch, Formal analysis, Investigation, Methodology, Writing - original draft, Writing - review and editing; Sydney K Vaughan, Data curation, Formal analysis, Writing - original draft, Writing - review and editing; Kerilyn Godbe, Formal analysis, Writing - review and editing; John Chappell, Resources, Writing - review and editing; Robert E Settlege, Formal analysis, Methodology, Writing - original draft, Writing - review and editing; Gregorio Valdez, Conceptualization, Resources, Data curation, Formal analysis, Supervision, Funding acquisition, Investigation, Methodology, Writing - original draft, Writing - review and editing

### Author ORCIDs

Ryan Castro  <https://orcid.org/0000-0002-2316-8039>  
 Thomas Taetzsch  <http://orcid.org/0000-0003-3257-1142>  
 Sydney K Vaughan  <https://orcid.org/0000-0002-3427-4654>  
 Robert E Settlege  <http://orcid.org/0000-0002-1354-7609>  
 Gregorio Valdez  <https://orcid.org/0000-0002-0375-4532>

### Ethics

Animal experimentation: All experiments were carried out under NIH guidelines and animal protocols approved by the Brown University (IACUC# 19-05-0013) and Virginia Tech (IACUC# 18-148 and 18-176) Institutional Animal Care and Use Committee.

### Decision letter and Author response

Decision letter <https://doi.org/10.7554/eLife.56935.sa1>  
 Author response <https://doi.org/10.7554/eLife.56935.sa2>

## Additional files

### Supplementary files

- Supplementary file 1. Genes with highly enriched expression in perisynaptic Schwann cells.
- Supplementary file 2. Primers used for cDNA preamplification and qPCR.
- Transparent reporting form

### Data availability

RNA-Seq data has been deposited in NCBI GEO and all other data is available in the main text or the supplementary materials. The GEO accession number for this dataset is GSE152774.

The following dataset was generated:

Author(s)	Year	Dataset title	Dataset URL	Database and Identifier
Castro R, Taetzsch T, Vaughan SK, Godbe K, Chappell	2020	Synaptic Schwann cells: specific labeling reveals unique cellular and molecular features	<a href="https://www.ncbi.nlm.nih.gov/geo/query/acc.cgi?acc=GSE152774">https://www.ncbi.nlm.nih.gov/geo/query/acc.cgi?acc=GSE152774</a>	NCBI Gene Expression Omnibus, GSE152774

J, Settlage RE, Valdez G

## References

- Anders S, Pyl PT, Huber W. 2015. HTSeq—a Python framework to work with high-throughput sequencing data. *Bioinformatics* **31**:166–169. DOI: <https://doi.org/10.1093/bioinformatics/btu638>, PMID: 25260700
- Aronesty E. 2013. Comparison of sequencing utility programs. *The Open Bioinformatics Journal* **7**:1–8. DOI: <https://doi.org/10.2174/1875036201307010001>
- Astrow SH, Son YJ, Thompson WJ. 1994. Differential neural regulation of a neuromuscular junction-associated antigen in muscle fibers and schwann cells. *Journal of Neurobiology* **25**:937–952. DOI: <https://doi.org/10.1002/neu.480250804>, PMID: 7525869
- Astrow SH, Qiang H, Ko CP. 1998. Perisynaptic schwann cells at neuromuscular junctions revealed by a novel monoclonal antibody. *Journal of Neurocytology* **27**:667–681. DOI: <https://doi.org/10.1023/a:1006916232627>, PMID: 10447241
- Barik A, Li L, Sathyamurthy A, Xiong WC, Mei L. 2016. Schwann cells in neuromuscular junction formation and maintenance. *Journal of Neuroscience* **36**:9770–9781. DOI: <https://doi.org/10.1523/JNEUROSCI.0174-16.2016>, PMID: 27656017
- Bergles DE, Jabs R, Steinhäuser C. 2010. Neuron-glia synapses in the brain. *Brain Research Reviews* **63**:130–137. DOI: <https://doi.org/10.1016/j.brainresrev.2009.12.003>, PMID: 20018210
- Birbrair A, Zhang T, Wang ZM, Messi ML, Enikolopov GN, Mintz A, Delbono O. 2013a. Role of pericytes in skeletal muscle regeneration and fat accumulation. *Stem Cells and Development* **22**:2298–2314. DOI: <https://doi.org/10.1089/scd.2012.0647>, PMID: 23517218
- Birbrair A, Zhang T, Wang ZM, Messi ML, Enikolopov GN, Mintz A, Delbono O. 2013b. Skeletal muscle pericyte subtypes differ in their differentiation potential. *Stem Cell Research* **10**:67–84. DOI: <https://doi.org/10.1016/j.scr.2012.09.003>, PMID: 23128780
- Boeke J. 1949. The sympathetic endformation, its synaptology, the interstitial cells, the periterminal network, and its bearing on the neurone theory discussion and critique. *Cells Tissues Organs* **8**:18–61. DOI: <https://doi.org/10.1159/000140398>
- Brill MS, Lichtman JW, Thompson W, Zuo Y, Misgeld T. 2011. Spatial constraints dictate glial territories at murine neuromuscular junctions. *Journal of Cell Biology* **195**:293–305. DOI: <https://doi.org/10.1083/jcb.201108005>
- Brockes JP, Fields KL, Raff MC. 1979. Studies on cultured rat schwann cells. I. establishment of purified populations from cultures of peripheral nerve. *Brain Research* **165**:105–118. DOI: [https://doi.org/10.1016/0006-8993\(79\)90048-9](https://doi.org/10.1016/0006-8993(79)90048-9), PMID: 371755
- Changeux JP, Kasai M, Lee CY. 1970. Use of a snake venom toxin to characterize the cholinergic receptor protein. *PNAS* **67**:1241–1247. DOI: <https://doi.org/10.1073/pnas.67.3.1241>, PMID: 5274453
- Cook JE. 1996. Spatial properties of retinal mosaics: an empirical evaluation of some existing measures. *Visual Neuroscience* **13**:15–30. DOI: <https://doi.org/10.1017/S09592523800007094>, PMID: 8730986
- Couteaux R. 1960. *The Structure and Function of Muscle*. Elsevier. DOI: <https://doi.org/10.1016/C2013-0-10402-3>
- Covault J, Sanes JR. 1986. Distribution of N-CAM in synaptic and extrasynaptic portions of developing and adult skeletal muscle. *The Journal of Cell Biology* **102**:716–730. DOI: <https://doi.org/10.1083/jcb.102.3.716>, PMID: 3512581
- Dalkin W, Taetzsch T, Valdez G. 2016. The fibular nerve injury method: a reliable assay to identify and test factors that repair neuromuscular junctions. *Journal of Visualized Experiments* **11**:54186. DOI: <https://doi.org/10.3791/54186>
- Darabid H, Arbour D, Robitaille R. 2013. Glial cells decipher synaptic competition at the mammalian neuromuscular junction. *Journal of Neuroscience* **33**:1297–1313. DOI: <https://doi.org/10.1523/JNEUROSCI.2935-12.2013>, PMID: 23345206
- Darabid H, Perez-Gonzalez AP, Robitaille R. 2014. Neuromuscular synaptogenesis: coordinating partners with multiple functions. *Nature Reviews Neuroscience* **15**:703–718. DOI: <https://doi.org/10.1038/nrn3821>, PMID: 25493308
- Darabid H, St-Pierre-See A, Robitaille R. 2018. Purinergic-Dependent glial regulation of synaptic plasticity of competing terminals and synapse elimination at the neuromuscular junction. *Cell Reports* **25**:2070–2082. DOI: <https://doi.org/10.1016/j.celrep.2018.10.075>, PMID: 30463006
- De Winter F, Vo T, Stam FJ, Wisman LA, Bär PR, Niclou SP, van Muiswinkel FL, Verhaagen J. 2006. The expression of the chemorepellent semaphorin 3A is selectively induced in terminal schwann cells of a subset of neuromuscular synapses that display limited anatomical plasticity and enhanced vulnerability in motor neuron disease. *Molecular and Cellular Neuroscience* **32**:102–117. DOI: <https://doi.org/10.1016/j.mcn.2006.03.002>, PMID: 16677822
- Deloulme JC, Raponi E, Gentil BJ, Bertacchi N, Marks A, Labourdette G, Baudier J. 2004. Nuclear expression of S100B in oligodendrocyte progenitor cells correlates with differentiation toward the oligodendroglial lineage and modulates oligodendrocytes maturation. *Molecular and Cellular Neuroscience* **27**:453–465. DOI: <https://doi.org/10.1016/j.mcn.2004.07.008>, PMID: 15555923

- Descarries LM**, Cai S, Robitaille R, Josephson EM, Morest DK. 1998. Localization and characterization of nitric oxide synthase at the frog neuromuscular junction. *Journal of Neurocytology* **27**:829–840. DOI: <https://doi.org/10.1023/a:1006907531778>, PMID: 10451429
- Fatt P**, Katz B. 1952. The electric activity of the motor end-plate. *Proc. R. Soc. London. Ser. B, Biol. Sci* **140**:183–186. DOI: <https://doi.org/10.1098/rspb.1952.0055>
- Feng Z**, Ko CP. 2008. Schwann cells promote synaptogenesis at the neuromuscular junction via transforming growth factor-beta1. *Journal of Neuroscience* **28**:9599–9609. DOI: <https://doi.org/10.1523/JNEUROSCI.2589-08.2008>, PMID: 18815246
- Filous AR**, Tran A, Howell CJ, Busch SA, Evans TA, Stallcup WB, Kang SH, Bergles DE, Lee SI, Levine JM, Silver J. 2014. Entrapment via synaptic-like connections between NG2 proteoglycan+ cells and dystrophic axons in the lesion plays a role in regeneration failure after spinal cord injury. *The Journal of Neuroscience* **34**:16369–16384. DOI: <https://doi.org/10.1523/JNEUROSCI.1309-14.2014>, PMID: 25471575
- Fox MA**, Umemori H. 2006. Seeking long-term relationship: axon and target communicate to organize synaptic differentiation. *Journal of Neurochemistry* **97**:1215–1231. DOI: <https://doi.org/10.1111/j.1471-4159.2006.03834.x>, PMID: 16638017
- Georgiou J**, Charlton MP. 1999. Non-myelin-forming perisynaptic schwann cells express protein zero and myelin-associated glycoprotein. *Glia* **27**:101–109. DOI: [https://doi.org/10.1002/\(SICI\)1098-1136\(199908\)27:2<101::AID-GLIA1>3.0.CO;2-H](https://doi.org/10.1002/(SICI)1098-1136(199908)27:2<101::AID-GLIA1>3.0.CO;2-H), PMID: 10417810
- Godfrey EW**, Nitkin RM, Wallace BG, Rubin LL, McMahan UJ. 1984. Components of Torpedo electric organ and muscle that cause aggregation of acetylcholine receptors on cultured muscle cells. *The Journal of Cell Biology* **99**:615–627. DOI: <https://doi.org/10.1083/jcb.99.2.615>, PMID: 6746740
- Gorlewicz A**, Włodarczyk J, Wilczek E, Gawlak M, Cabaj A, Majczynski H, Nestorowicz K, Herbiak MA, Grieb P, Ślawinska U, Kaczmarek L, Wilczynski GM. 2009. CD44 is expressed in non-myelinating schwann cells of the adult rat, and may play a role in neurodegeneration-induced glial plasticity at the neuromuscular junction. *Neurobiology of Disease* **34**:245–258. DOI: <https://doi.org/10.1016/j.nbd.2009.01.011>
- Griffin JW**, Thompson WJ. 2008. Biology and pathology of nonmyelinating schwann cells. *Glia* **56**:1518–1531. DOI: <https://doi.org/10.1002/glia.20778>, PMID: 18803315
- Gurney ME**, Pu H, Chiu AY, Dal Canto MC, Polchow CY, Alexander DD, Caliendo J, Hentati A, Kwon YW, Deng HX. 1994. Motor neuron degeneration in mice that express a human cu,zn superoxide dismutase mutation. *Science* **264**:1772–1775. DOI: <https://doi.org/10.1126/science.8209258>, PMID: 8209258
- Hachem S**, Aguirre A, Vives V, Marks A, Gallo V, Legraverend C. 2005. Spatial and temporal expression of S100B in cells of oligodendrocyte lineage. *Glia* **51**:81–97. DOI: <https://doi.org/10.1002/glia.20184>, PMID: 15782413
- Heredia DJ**, Feng CY, Agarwal A, Nennecker K, Hennig GW, Gould TW. 2018. Postnatal restriction of Activity-Induced Ca<sup>2+</sup> Responses to Schwann Cells at the Neuromuscular Junction Are Caused by the Proximo-Distal Loss of Axonal Synaptic Vesicles during Development. *The Journal of Neuroscience* **38**:8650–8665. DOI: <https://doi.org/10.1523/JNEUROSCI.0956-18.2018>, PMID: 30143570
- Hess DM**, Scott MO, Potluri S, Pitts EV, Cisterni C, Balice-Gordon RJ. 2007. Localization of TrkC to schwann cells and effects of neurotrophin-3 signaling at neuromuscular synapses. *The Journal of Comparative Neurology* **501**:465–482. DOI: <https://doi.org/10.1002/cne.21163>, PMID: 17278135
- Heuser JE**, Reese TS. 1973. Evidence for recycling of synaptic vesicle membrane during transmitter release at the frog neuromuscular junction. *The Journal of Cell Biology* **57**:315–344. DOI: <https://doi.org/10.1083/jcb.57.2.315>, PMID: 4348786
- Jahromi BS**, Robitaille R, Charlton MP. 1992. Transmitter release increases intracellular calcium in Perisynaptic schwann cells in situ. *Neuron* **8**:1069–1077. DOI: [https://doi.org/10.1016/0896-6273\(92\)90128-Z](https://doi.org/10.1016/0896-6273(92)90128-Z), PMID: 1351731
- Jäkel S**, Dimou L. 2017. Glial cells and their function in the adult brain: a journey through the history of their ablation. *Frontiers in Cellular Neuroscience* **11**:24. DOI: <https://doi.org/10.3389/fncel.2017.00024>, PMID: 28243193
- Jennings CG**, Dyer SM, Burden SJ. 1993. Muscle-specific trk-related receptor with a kringle domain defines a distinct class of receptor tyrosine kinases. *PNAS* **90**:2895–2899. DOI: <https://doi.org/10.1073/pnas.90.7.2895>, PMID: 8385349
- Kang H**, Tian L, Son YJ, Zuo Y, Procaccino D, Love F, Hayworth C, Trachtenberg J, Mikesch M, Sutton L, Ponomareva O, Mignone J, Enikolopov G, Rimer M, Thompson W. 2007. Regulation of the intermediate filament protein nestin at rodent neuromuscular junctions by innervation and activity. *Journal of Neuroscience* **27**:5948–5957. DOI: <https://doi.org/10.1523/JNEUROSCI.0621-07.2007>, PMID: 17537965
- Katz B**, Miledi R. 1966. Input-output relation of a single synapse. *Nature* **212**:1242–1245. DOI: <https://doi.org/10.1038/2121242a0>, PMID: 21090453
- Katz B**, Miledi R. 1967. A study of synaptic transmission in the absence of nerve impulses. *The Journal of Physiology* **192**:407–436. DOI: <https://doi.org/10.1113/jphysiol.1967.sp008307>, PMID: 4383089
- Kim D**, Paggi JM, Park C, Bennett C, Salzberg SL. 2019. Graph-based genome alignment and genotyping with HISAT2 and HISAT-genotype. *Nature Biotechnology* **37**:907–915. DOI: <https://doi.org/10.1038/s41587-019-0201-4>, PMID: 31375807
- Ko CP**, Robitaille R. 2015. Perisynaptic schwann cells at the neuromuscular synapse: adaptable, multitasking glial cells. *Cold Spring Harbor Perspectives in Biology* **7**:a020503. DOI: <https://doi.org/10.1101/cshperspect.a020503>, PMID: 26430218



- Koirala S**, Qiang H, Ko CP. 2000. Reciprocal interactions between perisynaptic schwann cells and regenerating nerve terminals at the frog neuromuscular junction. *Journal of Neurobiology* **44**:343–360. DOI: [https://doi.org/10.1002/1097-4695\(20000905\)44:3<343::AID-NEU5>3.0.CO;2-O](https://doi.org/10.1002/1097-4695(20000905)44:3<343::AID-NEU5>3.0.CO;2-O), PMID: 10942887
- Kong Y**. 2011. Btrim: a fast, lightweight adapter and quality trimming program for next-generation sequencing technologies. *Genomics* **98**:152–153. DOI: <https://doi.org/10.1016/j.ygeno.2011.05.009>, PMID: 21651976
- Lee YI**, Thompson WJ, Harlow ML. 2017. Schwann cells participate in synapse elimination at the developing neuromuscular junction. *Current Opinion in Neurobiology* **47**:176–181. DOI: <https://doi.org/10.1016/j.conb.2017.10.010>, PMID: 29121585
- Love MI**, Huber W, Anders S. 2014. Moderated estimation of fold change and dispersion for RNA-seq data with DESeq2. *Genome Biology* **15**:550. DOI: <https://doi.org/10.1186/s13059-014-0550-8>, PMID: 25516281
- Love FM**, Thompson WJ. 1998. Schwann cells proliferate at rat neuromuscular junctions during development and regeneration. *The Journal of Neuroscience* **18**:9376–9385. DOI: <https://doi.org/10.1523/JNEUROSCI.18-22-09376.1998>, PMID: 9801376
- Lwebuga-Mukasa JS**, Lappi S, Taylor P. 1976. Molecular forms of acetylcholinesterase from *Torpedo californica*: their relationship to synaptic membranes. *Biochemistry* **15**:1425–1434. DOI: <https://doi.org/10.1021/bi00652a012>, PMID: 177042
- Matthias K**, Kirchoff F, Seifert G, Hüttmann K, Matyash M, Kettenmann H, Steinhäuser C. 2003. Segregated expression of AMPA-type glutamate receptors and glutamate transporters defines distinct astrocyte populations in the mouse Hippocampus. *The Journal of Neuroscience* **23**:1750–1758. DOI: <https://doi.org/10.1523/JNEUROSCI.23-05-01750.2003>, PMID: 12629179
- Miledi R**, Slater CR. 1968. Electrophysiology and electron-microscopy of rat neuromuscular junctions after nerve degeneration. *Proc. R. Soc. London. Ser. B. Biol. Sci* **169**:289–306. DOI: <https://doi.org/10.1098/rspb.1968.0012>
- Miledi R**, Slater CR. 1970. On the degeneration of rat neuromuscular junctions after nerve section. *The Journal of Physiology* **207**:507–528. DOI: <https://doi.org/10.1113/jphysiol.1970.sp009076>, PMID: 5499034
- Moloney EB**, de Winter F, Verhaagen J. 2014. ALS as a distal axonopathy: molecular mechanisms affecting neuromuscular junction stability in the presymptomatic stages of the disease. *Frontiers in Neuroscience* **8**:252. DOI: <https://doi.org/10.3389/fnins.2014.00252>, PMID: 25177267
- Morris JK**, Lin W, Hauser C, Marchuk Y, Getman D, Lee KF. 1999. Rescue of the cardiac defect in ErbB2 mutant mice reveals essential roles of ErbB2 in peripheral nervous system development. *Neuron* **23**:273–283. DOI: [https://doi.org/10.1016/S0896-6273\(00\)80779-5](https://doi.org/10.1016/S0896-6273(00)80779-5), PMID: 10399934
- Moshrefi-Ravasdjani B**, Dublin P, Seifert G, Jennissen K, Steinhäuser C, Kafitz KW, Rose CR. 2017. Changes in the proliferative capacity of NG2 cell subpopulations during postnatal development of the mouse Hippocampus. *Brain Structure and Function* **222**:831–847. DOI: <https://doi.org/10.1007/s00429-016-1249-2>, PMID: 27306788
- Mozer BA**, Sandstrom DJ. 2012. *Drosophila* neuroligin 1 regulates synaptic growth and function in response to activity and phosphoinositide-3-kinase. *Molecular and Cellular Neuroscience* **51**:89–100. DOI: <https://doi.org/10.1016/j.mcn.2012.08.010>, PMID: 22954894
- Musarella M**, Alcaraz G, Caillol G, Boudier JL, Couraud F, Autillo-Touati A. 2006. Expression of Nav1.6 sodium channels by Schwann cells at neuromuscular junctions: role in the motor endplate disease phenotype. *Glia* **53**:13–23. DOI: <https://doi.org/10.1002/glia.20252>, PMID: 16078241
- Nitkin RM**, Smith MA, Magill C, Fallon JR, Yao YM, Wallace BG, McMahan UJ. 1987. Identification of Agrin, a synaptic organizing protein from *Torpedo electric organ*. *The Journal of Cell Biology* **105**:2471–2478. DOI: <https://doi.org/10.1083/jcb.105.6.2471>, PMID: 2826489
- O'Malley JP**, Waran MT, Balice-Gordon RJ. 1999. In vivo observations of terminal schwann cells at normal, denervated, and reinnervated mouse neuromuscular junctions. *Journal of Neurobiology* **38**:270–286. DOI: [https://doi.org/10.1002/\(SICI\)1097-4695\(19990205\)38:2<270::AID-NEU9>3.0.CO;2-F](https://doi.org/10.1002/(SICI)1097-4695(19990205)38:2<270::AID-NEU9>3.0.CO;2-F), PMID: 10022572
- Park SY**, Jang SY, Shin YK, Jung DK, Yoon BA, Kim JK, Jo YR, Lee HJ, Park HT. 2017. The scaffolding protein, Grb2-associated Binder-1, in skeletal muscles and terminal schwann cells regulates postnatal neuromuscular synapse maturation. *Experimental Neurobiology* **26**:141–150. DOI: <https://doi.org/10.5607/en.2017.26.3.141>, PMID: 28680299
- Peng F**, Yao H, Bai X, Zhu X, Reiner BC, Beazely M, Funa K, Xiong H, Buch S. 2010. Platelet-derived growth factor-mediated induction of the synaptic plasticity gene *arc/Arg3.1*. *Journal of Biological Chemistry* **285**:21615–21624. DOI: <https://doi.org/10.1074/jbc.M110.107003>, PMID: 20452974
- Peper K**, Dreyer F, Sandri C, Akert K, Moor H. 1974. Structure and ultrastructure of the frog motor endplate a freeze-etching study. *Cell and Tissue Research* **149**:437–455. DOI: <https://doi.org/10.1007/BF00223024>, PMID: 4546545
- Perez VJ**, Moore BW. 1968. Wallerian degeneration in rabbit tibial nerve: changes in amounts of the S-100 protein. *Journal of Neurochemistry* **15**:971–977. DOI: <https://doi.org/10.1111/j.1471-4159.1968.tb11640.x>, PMID: 5682514
- Personius KE**, Slusher BS, Udin SB. 2016. Neuromuscular NMDA receptors modulate developmental synapse elimination. *The Journal of Neuroscience* **36**:8783–8789. DOI: <https://doi.org/10.1523/JNEUROSCI.1181-16.2016>, PMID: 27559162
- Petrov KA**, Girard E, Nikitashina AD, Colasante C, Bernard V, Nurullin L, Leroy J, Samigullin D, Colak O, Nikolsky E, Plaud B, Krejci E. 2014. Schwann cells sense and control acetylcholine spillover at the neuromuscular junction by  $\alpha 7$  nicotinic receptors and butyrylcholinesterase. *Journal of Neuroscience* **34**:11870–11883. DOI: <https://doi.org/10.1523/JNEUROSCI.0329-14.2014>, PMID: 25186736

- Pinard A**, Lévesque S, Vallée J, Robitaille R. 2003. Glutamatergic modulation of synaptic plasticity at a PNS vertebrate cholinergic synapse. *European Journal of Neuroscience* **18**:3241–3250. DOI: <https://doi.org/10.1111/j.1460-9568.2003.03028.x>, PMID: 14686898
- Platel JC**, Gordon V, Heintz T, Bordey A. 2009. GFAP-GFP neural progenitors are antigenically homogeneous and anchored in their enclosed mosaic niche. *Glia* **57**:66–78. DOI: <https://doi.org/10.1002/glia.20735>, PMID: 18661547
- Porter S**, Froehner SC. 1983. Characterization and localization of the mr = 43,000 proteins associated with acetylcholine receptor-rich membranes. *The Journal of Biological Chemistry* **258**:10034–10040. PMID: 6885756
- Rafuse VF**, Polo-Parada L, Landmesser LT. 2000. Structural and functional alterations of neuromuscular junctions in NCAM-deficient mice. *The Journal of Neuroscience* **20**:6529–6539. DOI: <https://doi.org/10.1523/JNEUROSCI.20-17-06529.2000>, PMID: 10964958
- Ranaivoson FM**, Turk LS, Ozgul S, von Daake S, Lopez N, Trobiani L, De Jaco A, Denissova N, Demeler B, Özkan E, Montelione GT, Comoletti D. 2019. A proteomic screen of neuronal Cell-Surface molecules reveals IgLONs as structurally conserved interaction modules at the synapse. *Structure* **27**:893–906. DOI: <https://doi.org/10.1016/j.str.2019.03.004>, PMID: 30956130
- Reddy LV**, Koirala S, Sugiura Y, Herrera AA, Ko CP. 2003. Glial cells maintain synaptic structure and function and promote development of the neuromuscular junction in vivo. *Neuron* **40**:563–580. DOI: [https://doi.org/10.1016/S0896-6273\(03\)00682-2](https://doi.org/10.1016/S0896-6273(03)00682-2), PMID: 14642280
- Reese BE**, Keeley PW. 2015. Design principles and developmental mechanisms underlying retinal mosaics. *Biological Reviews* **90**:854–876. DOI: <https://doi.org/10.1111/brv.12139>, PMID: 25109780
- Reist NE**, Smith SJ. 1992. Neurally evoked calcium transients in terminal schwann cells at the neuromuscular junction. *PNAS* **89**:7625–7629. DOI: <https://doi.org/10.1073/pnas.89.16.7625>, PMID: 1502174
- Reynolds ML**, Woolf CJ. 1992. Terminal schwann cells elaborate extensive processes following denervation of the motor endplate. *Journal of Neurocytology* **21**:50–66. DOI: <https://doi.org/10.1007/BF01206897>, PMID: 1346630
- Riethmacher D**, Sonnenberg-Riethmacher E, Brinkmann V, Yamaai T, Lewin GR, Birchmeier C. 1997. Severe neuropathies in mice with targeted mutations in the ErbB3 receptor. *Nature* **389**:725–730. DOI: <https://doi.org/10.1038/39593>, PMID: 9338783
- Robertson JD**. 1956. The ultrastructure of a reptilian myoneural junction. *The Journal of Biophysical and Biochemical Cytology* **2**:381–394. DOI: <https://doi.org/10.1083/jcb.2.4.381>, PMID: 13357502
- Robitaille R**. 1995. Purinergic receptors and their activation by endogenous purines at Perisynaptic glial cells of the frog neuromuscular junction. *The Journal of Neuroscience* **15**:7121–7131. DOI: <https://doi.org/10.1523/JNEUROSCI.15-11-07121.1995>, PMID: 7472466
- Robitaille R**, Bourque MJ, Vandaele S. 1996. Localization of L-type Ca<sup>2+</sup> channels at Perisynaptic glial cells of the frog neuromuscular junction. *The Journal of Neuroscience* **16**:148–158. DOI: <https://doi.org/10.1523/JNEUROSCI.16-01-00148.1996>, PMID: 8613781
- Robitaille R**, Jahromi BS, Charlton MP. 1997. Muscarinic Ca<sup>2+</sup> responses resistant to muscarinic antagonists at Perisynaptic schwann cells of the frog neuromuscular junction. *The Journal of Physiology* **504**:337–347. DOI: <https://doi.org/10.1111/j.1469-7793.1997.337be.x>, PMID: 9365908
- Rochon D**, Rousse I, Robitaille R. 2001. Synapse-glia interactions at the mammalian neuromuscular junction. *The Journal of Neuroscience* **21**:3819–3829. DOI: <https://doi.org/10.1523/JNEUROSCI.21-11-03819.2001>, PMID: 11356870
- Sanes JR**, Lichtman JW. 1999. Development of the vertebrate neuromuscular junction. *Annual Review of Neuroscience* **22**:389–442. DOI: <https://doi.org/10.1146/annurev.neuro.22.1.389>, PMID: 10202544
- Sanes JR**, Lichtman JW. 2001. Induction, assembly, maturation and maintenance of a postsynaptic apparatus. *Nature Reviews Neuroscience* **2**:791–805. DOI: <https://doi.org/10.1038/35097557>, PMID: 11715056
- Sealock R**, Murnane AA, Paulin D, Froehner SC. 1989. Immunochemical identification of desmin in Torpedo postsynaptic membranes and at the rat neuromuscular junction. *Synapse* **3**:315–324. DOI: <https://doi.org/10.1002/syn.890030404>, PMID: 2740991
- Shapiro L**, Love J, Colman DR. 2007. Adhesion molecules in the nervous system: structural insights into function and diversity. *Annual Review of Neuroscience* **30**:451–474. DOI: <https://doi.org/10.1146/annurev.neuro.29.051605.113034>, PMID: 17600523
- Smith IW**, Mikes M, Lee Y, Thompson WJ. 2013. Terminal schwann cells participate in the competition underlying neuromuscular synapse elimination. *Journal of Neuroscience* **33**:17724–17736. DOI: <https://doi.org/10.1523/JNEUROSCI.3339-13.2013>, PMID: 24198364
- Sobel A**, Weber M, Changeux JP. 1977. Large-scale purification of the acetylcholine-receptor protein in its membrane-bound and detergent-extracted forms from Torpedo marmorata electric organ. *European Journal of Biochemistry* **80**:215–224. DOI: <https://doi.org/10.1111/j.1432-1033.1977.tb11874.x>, PMID: 923574
- Sobel A**, Hofler J, Heidmann T, Changeux JP. 1979. Structural and functional properties of the acetylcholine regulator. *Advances in Cytopharmacology* **3**:191–196. PMID: 382784
- Son YJ**, Thompson WJ. 1995. Schwann cell processes guide regeneration of peripheral axons. *Neuron* **14**:125–132. DOI: [https://doi.org/10.1016/0896-6273\(95\)90246-5](https://doi.org/10.1016/0896-6273(95)90246-5), PMID: 7826630
- Stallcup WB**. 1981. The NG2 antigen, a putative lineage marker: immunofluorescent localization in primary cultures of rat brain. *Developmental Biology* **83**:154–165. DOI: [https://doi.org/10.1016/S0012-1606\(81\)80018-8](https://doi.org/10.1016/S0012-1606(81)80018-8), PMID: 7016634
- Trachtenberg JT**, Thompson WJ. 1996. Schwann cell apoptosis at developing neuromuscular junctions is regulated by glial growth factor. *Nature* **379**:174–177. DOI: <https://doi.org/10.1038/379174a0>, PMID: 8538769

- Trachtenberg JT**, Thompson WJ. 1997. Nerve terminal withdrawal from rat neuromuscular junctions induced by neuregulin and schwann cells. *The Journal of Neuroscience* **17**:6243–6255. DOI: <https://doi.org/10.1523/JNEUROSCI.17-16-06243.1997>, PMID: 9236235
- Vives V**, Alonso G, Solal AC, Joubert D, Legraverend C. 2003. Visualization of S100B-positive neurons and Glia in the central nervous system of EGFP transgenic mice. *The Journal of Comparative Neurology* **457**:404–419. DOI: <https://doi.org/10.1002/cne.10552>, PMID: 12561079
- Wassle H**, Riemann HJ. 1978. The mosaic of Nhtman,erve cells in the mammalian retina. *Proc. R. Soc. London - Biol. Sci* **200**:441–461. DOI: <https://doi.org/10.1098/rspb.1978.0026>
- Woldeyesus MT**, Britsch S, Riethmacher D, Xu L, Sonnenberg-Riethmacher E, Abou-Rebyeh F, Harvey R, Caroni P, Birchmeier C. 1999. Peripheral nervous system defects in erbB2 mutants following genetic rescue of heart development. *Genes & Development* **13**:2538–2548. DOI: <https://doi.org/10.1101/gad.13.19.2538>, PMID: 10521398
- Wright MC**, Potluri S, Wang X, Dentcheva E, Gautam D, Tessler A, Wess J, Rich MM, Son YJ. 2009. Distinct muscarinic acetylcholine receptor subtypes contribute to stability and growth, but not compensatory plasticity, of neuromuscular synapses. *Journal of Neuroscience* **29**:14942–14955. DOI: <https://doi.org/10.1523/JNEUROSCI.2276-09.2009>, PMID: 19940190
- Yang JF**, Cao G, Koirala S, Reddy LV, Ko CP. 2001. Schwann cells express active agrin and enhance aggregation of acetylcholine receptors on muscle fibers. *The Journal of Neuroscience* **21**:9572–9584. DOI: <https://doi.org/10.1523/JNEUROSCI.21-24-09572.2001>, PMID: 11739568
- Young P**, Nie J, Wang X, McGlade CJ, Rich MM, Feng G. 2005. LNX1 is a perisynaptic schwann cell specific E3 ubiquitin ligase that interacts with ErbB2. *Molecular and Cellular Neuroscience* **30**:238–248. DOI: <https://doi.org/10.1016/j.mcn.2005.07.015>, PMID: 16122940
- Zhu X**, Bergles DE, Nishiyama A. 2008. NG2 cells generate both oligodendrocytes and gray matter astrocytes. *Development* **135**:145–157. DOI: <https://doi.org/10.1242/dev.004895>, PMID: 18045844
- Zuo Y**, Lubischer JL, Kang H, Tian L, Mikesh M, Marks A, Scofield VL, Maika S, Newman C, Krieg P, Thompson WJ. 2004. Fluorescent proteins expressed in mouse transgenic lines mark subsets of Glia, neurons, macrophages, and dendritic cells for vital examination. *Journal of Neuroscience* **24**:10999–11009. DOI: <https://doi.org/10.1523/JNEUROSCI.3934-04.2004>, PMID: 15590915